▌**Actinide Magnetism** |*Hot Paper*|

Spectroscopic Determination of the Electronic Structure of a Uranium Single-Ion Magnet

Joana T. Coutinho,[a] Mauro Perfetti,[b, c] José J. Baldoví,[d] Maria A. Antunes,[a] Philipp P. Hallmen,[b] Heiko Bamberger,[b] Iris Crassee,[e] Milan Orlita,[e, f] Manuel Almeida,[a] Joris van Slageren,*[b] and Laura C. J. Pereira*[a]

Abstract: Early actinide ions have large spin-orbit couplings and crystal field interactions, leading to large anisotropies. The success in using actinides as single-molecule magnets has so far been modest, underlining the need for rational strategies. Indeed, the electronic structure of actinide single-molecule magnets and its relation to their magnetic proper-ties remains largely unexplored. A uranium(III) single-mole-cule magnet, [U^{III}\{SiMe$_2$NPh\}$_3$-tacn)(OPPh$_3$)] (tacn = 1,4,7-tria-zacyclononane), has been investigated by means of a combi-nation of magnetic, spectroscopic and theoretical methods to elucidate the origin of its static and dynamic magnetic properties.

Introduction

The slow magnetic relaxation in f-element complexes, especial-ly those of the lanthanides, has been the subject of intense in-vestigation over the past 15 years.[1–4] This research was partly driven by the vision that such complexes, with single-molecule magnet (SMM) behaviour, might one day be used to store in-formation at a molecular level. Since the original publication on the first single-ion magnet (NBu$_4$)[Tb(Pc)$_2$] (H$_2$Pc = phthalo-cyanine),[5] the reported effective energy barriers have in-creased from 330 to about 1800 K.[6–8] Importantly, these last two years have seen the increase in the hysteresis blocking temperature achieving values close to the boiling point of ni-trogen (60 K)[7] and even above at 80 K.[8] These successes were achieved by following strategies of careful tailoring of the crys-tal field[6–9] or by the use of radical bridging ligands resulting in strongly coupled polynuclear species.[10–13] The former ap-proach may not be very robust against small structural changes such as those experienced upon molecular surface deposition, as required for device development. The realization of the latter approach is challenging and often results in highly reactive species.

Actinides are in this respect a valuable alternative because they possess stronger spin-orbit coupling and ligand field in-teractions and thus potentially larger magnetic anisotropies compared to those of lanthanides. Also, their comparative study with lanthanides may provide important clues to under-stand the relaxation mechanisms. Moreover, actinides allow for much stronger exchange interactions with neighbouring spin centres, especially those of transition metals,[14–17] which may suppress under barrier tunnelling processes. These stronger metal–ligand interactions arise because 5f orbitals have larger radial extensions than those of the 4f orbitals, increasing the covalency of metal–ligand interactions.[3, 18, 19] On the one hand, these predictions were borne out by several U^V-Mn^{II} systems that feature substantial coercivities in their magnetic hysteresis curves.[20–23] On the other hand, the single-ion properties of pure 5f-based single-molecule magnets have been somewhat disappointing, with effective energy barriers not surpassing 50 K.[3] Clearly, under barrier relaxation, by direct and Raman processes, effectively short-cuts the energy barrier created by crystal field splitting of the lowest multiplet. Presently, it is un-clear why the Orbach process of magnetization relaxation ap-pears to be less effective in 5f complexes,[3] and detailed ex-perimental and theoretical investigations of the electronic structure and magnetic properties of 5f complexes are thus es-sential. Such a comprehensive study on a series of uranium(V) complexes has been recently reported,[24] which combined

[a] Dr. J. T. Coutinho, Dr. M. A. Antunes, Prof. M. Almeida, Dr. L. C. J. Pereira
Center for Nuclear Sciences and Technologies (C2TN)
Instituto Superior Técnico, Universidade de Lisboa
Estrada Nacional 10, 2695-066 Bobadela LRS (Portugal)
E-mail: lpereira@ctn.tecnico.ulisboa.pt

[b] Dr. M. Perfetti, P. P. Hallmen, H. Bamberger, Prof. J. van Slageren
Institut für Physikalische Chemie, Universität Stuttgart
Pfaffenwaldring 55, 70569 Stuttgart (Germany)
E-mail: slageren@ipc.uni-stuttgart.de

[c] Dr. M. Perfetti
Department of Chemistry, University of Copenhagen
Universitetsparken 5, 2100 Copenhagen (Denmark)

[d] Dr. J. J. Baldoví
Max Planck Institute for the Structure and Dynamics of Matter
Luruper Chaussee 149, 22761 Hamburg (Germany)

[e] Dr. I. Crassee, Dr. M. Orlita
Laboratoire National des Champs Magnétiques Intenses
CNRS-UGA-UPS-INSA-EMFL
25 Avenue des Martyrs, 38042 Grenoble (France)

[f] Dr. M. Orlita
Institute of Physics, Charles University
Ke Karlovu 5, 12116 Praha 2 (Czech Republic)

Supporting Information and the ORCID identification number(s) for the author(s) of this article can be found under:
https://doi.org/10.1002/chem.201805090.

electronic absorption and EPR measurements with ab initio calculations. However, the majority of actinide-based single-molecule magnets are based on uranium(III), a Kramers ion with a large total angular momentum ground state ($5f^3$, ground $J = 9/2$). Detailed studies of similar scope of molecular U^{III} compounds are unknown to us, with the exception of an optical study of the single-ion magnet $U(Tp)_3$ (Tp = trispyrazolylborate).[25]

In 2015, some of us reported the study of a trivalent uranium compound, $[U^{III}(\{SiMe_2NPh\}_3\text{-tacn})]$ (tacn = 1,4,7-triazacyclononane) (1), that has an equatorial charge distribution around the uranium ion.[26] This system was found to be a rare example of a mononuclear U^{III} compound that does not exhibit slow relaxation of the magnetization down to 1.7 K, contrary to previous expectations.[27] To achieve slow relaxation and taking into consideration that in U^{III} the largest values of the total angular momentum quantum number, m_J values can be stabilized when the magnetic centre is placed in an axially elongated ligand field,[28–30] we decided to study a related compound, $[U^{III}(\{SiMe_2NPh\}_3\text{-tacn})(OPPh_3)]$ (2), in which the coordination environment of 1 was modified by adding an axial $OPPh_3$ ligand while maintaining its oxidation state. The protection of the axial coordination position by the phenyl groups prevents the approach of the $OPPh_3$ ligand to the U atom. This was intended to promote the SMM characteristics to the new complex 2.

Here we report the synthesis and a detailed study of 2, which indeed shows SMM properties and for which one of us previously presented preliminary results.[31] We present a detailed experimental and theoretical study of its electronic structure employing a range of spectroscopic studies, including high-frequency electron paramagnetic resonance (HFEPR) spectroscopy, far-infrared (FIR) spectroscopy and magnetic circular dichroism (MCD) spectroscopy, complemented by theoretical ab initio calculations and crystal field modelling using the full Hamiltonian.

Results and Discussion

Synthesis and structural characterization

Compound 2 (see the Experimental Section) crystallizes in the orthorhombic space group $P2_12_12_1$, with two molecules of toluene incorporated into the crystal lattice.[31] The U^{III} ion is in a capped trigonal prismatic coordination environment (Figure 1). The two triangular faces are individually defined by the three amido (N4, N5 and N6) and the three amino (N1, N2 and N3) nitrogen atoms of the ancillary ligand. The $OPPh_3$ ligand is located axially and caps the triangular face defined by the amido atoms (the angle between the U—O axis and the normal to the plane defined by N4, N5 and N6 is 1°) (see also Figure S1 and Table S1 in Supporting Information).

Compared to its precursor $[U^{III}(\{SiMe_2NPh\}_3\text{-tacn})]$ (1),[32] which also displays a trigonal prismatic geometry, the coordination of an axial ligand in compound 2 results in a shorter distance of the uranium ion to the amido plane (the metal centre is lying just below the amido plane at 0.52 and 0.27 Å
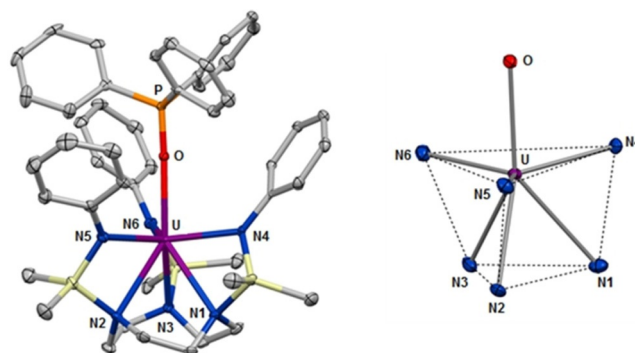

Figure 1. Molecular structure and coordination geometry of $[U^{III}(\{SiMe_2NPh\}_3\text{-tacn})(OPPh_3)]\cdot 2\,C_7H_8$. Ellipsoids are displayed at a probability level of 50%. Hydrogen atoms and solvent molecules are omitted for clarity. Selected bond lengths [Å] and angles [°]: U—N1 2.750(3), U—N2 2.785(3), U—N3 2.762(3), U—N4 2.454(3), U—N5 2.436(3), U—N6 2.468(3), U—O 2.483(2), N4-U-N5 117.35(9), N4-U-N6 120.56(9), N5-U-N6 118.43(9), U-O-P 176.96(14).

in 1 and 2, respectively) and in a more distorted coordination geometry, as seen by the twist angle between the trigonal faces that increases from 0.8° in 1 to 12.4° in 2. The bond lengths U—N(amido) [2.436(2), 2.454(3) and 2.468(3) Å] and U—N(amino) [2.750(3), 2.762(3) and 2.785(3) Å] in 2 are longer by about 0.1 Å than those in 1 (2.35(2) and 2.66(2) Å on average, respectively), as expected for a compound with a higher coordination number. The bond length U—O [2.483(2) Å] is longer than the ones found for reported trivalent uranium complexes bearing the $OPPh_3$ ligand.[33–36] This may be due to geometric constraints imposed by the three phenyl groups of the tacn ligand; the orientation around the axial position of which does not allow the $OPPh_3$ ligand to be closer to the metal centre. As expected, the U-O-P angle is almost linear [176.96(14)]. The O—P bond length is 1.508(2) Å, which is comparable to those observed in free $OPPh_3$ (an average value of 1.494 Å from 256 crystal structures of the Cambridge Structural Database (CSD; version 5.36, Nov 2014) that contain free $OPPh_3$) and in the related U^{III} compounds mentioned above, for which the O—P distances range from 1.491 to 1.520 Å.[33–36]

Magnetic properties

The temperature dependence of the magnetic susceptibility temperature product (χT) of 2 measured between 4 and 300 K, under a static magnetic field of 2 kOe, reveals a gradual decrease of χT from 1.13 cm^3 K mol^{-1} at 300 K to 0.53 cm^3 K mol^{-1} at 4 K (Figure 2). This decrease results from a progressive depopulation of the low-lying crystal field states of the uranium ion.[37] The χT value at room temperature is lower than the expected value of 1.64 cm^3 K mol^{-1} for a non-interacting U^{3+} ion ($5f^3$, $^4I_{9/2}$) but well within the range observed for U^{III} coordination compounds, which indicates that not all levels are populated at 300 K.[38–40] The magnetic hysteresis curve recorded on the same sample with a field sweep rate of 20 Oe s^{-1} shows no appreciable coercivity down to a temperature of 1.7 K (inset of Figure 2), as regularly observed for uranium compounds, for which the opening of hysteresis is typically observed only below 1.5 K.[26,41]
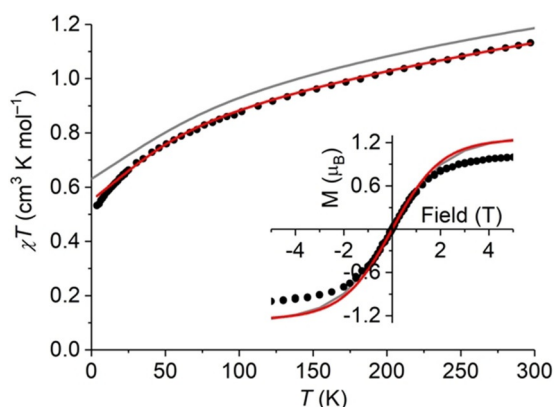
Figure 2. Experimental (symbols), fitted (red line) and ab initio calculated (grey line) temperature dependence of the magnetic susceptibility temperature product (χT) of **2** at 2 kOe. The inset shows the magnetic hysteresis curve recorded on the same sample at 1.7 K and a field sweep rate of 20 Oe s^{-1}, as well as the ab initio calculated curve.

Information on the magnetization dynamics was obtained by measurement of the ac susceptibility at low temperatures (1.6–10 K) and different frequencies, with an ac field of 5 Oe and in 0 and 2 kOe static fields (Figure S2, Supporting Information). In contrast to the magnetic behaviour of compound **1** (for which no evidence for slow magnetic relaxation was observed),[26] compound **2** showed evidence for slow relaxation of magnetization below 5 K, with frequency-dependent maxima in both real, χ'_{ac}, and imaginary, χ''_{ac}, components of susceptibility, even in zero static field. Application of a static field slows down the relaxation rate, and at 1.7 K, the maximum relaxation time is observed at 2 kOe (Figure S3, Supporting Information). For a quantitative analysis, the frequency dependence of the ac susceptibility at different temperatures was measured in the range of 10 Hz to 10 kHz under this optimum external field of $H_{dc} = 2$ kOe (Figure 3). The Argand plots derived from these data (Figure S4, Supporting Information) were fitted by using a generalized Debye model (see Supporting Information). The nearly semicircular and symmetrical shape of these plots, which are well-fitted considering a narrow distribution of relaxation times ($0.077 \leq \alpha \leq 0.028$) (Table S2, Supporting Information), are consistent with a single magnetization relaxation process occurring, as previously observed for other uranium SMMs.[26,41,42] The product of the temperature and the difference between adiabatic (χ_S), and isothermal (χ_T) susceptibilities ($\chi_S - \chi_T$)T is about half of $\chi_{dc}T$, in which χ_{dc} is the susceptibility determined from the dc susceptibility measurement. This suggests that the slow relaxation process is relevant for about half the sample.

Fits of the temperature dependence of the relaxation time τ to a Arrhenius law, $\tau = \tau_0 \times \exp(U_{eff}/k_B T)$, yielded pre-exponential factors (τ_0) of $1.7(1) \times 10^{-7}$ s and $7.8(3) \times 10^{-8}$ s and effective energy barriers (U_{eff}) of 21.9(7) K and 25.1(3.8) K under 0 and 2 kOe static fields, respectively (Figure 4a). Although determined for a very limited range of temperatures, these values are in agreement with previously reported effective barriers for mononuclear U^{III} complexes.[18,41–44] However, the curved nature of the Arrhenius plot implies that a single Orbach process
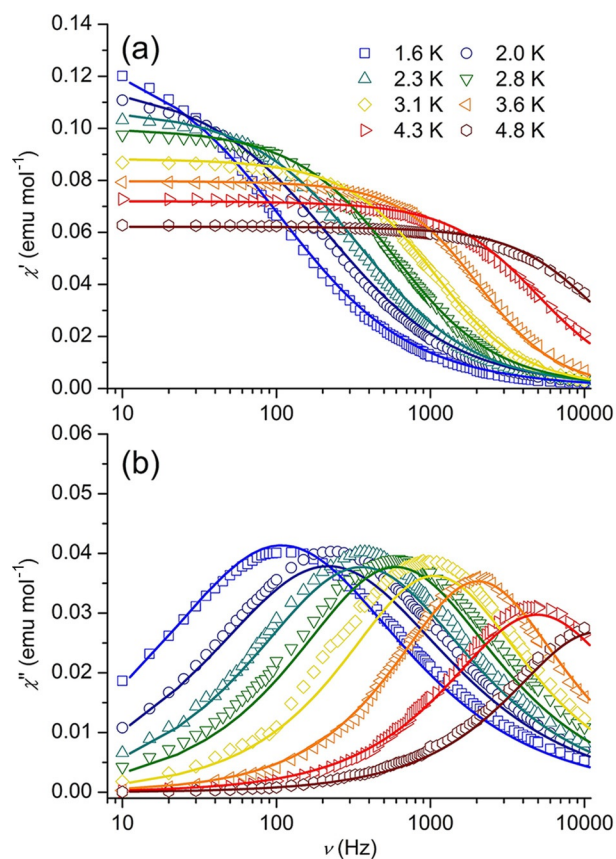

Figure 3. Frequency dependence of the in-phase (a) and out-of-phase (b) components of the ac susceptibility of **2** in the 1.6–4.8 K temperature range in a static field on $H_{dc} = 2$ kOe.
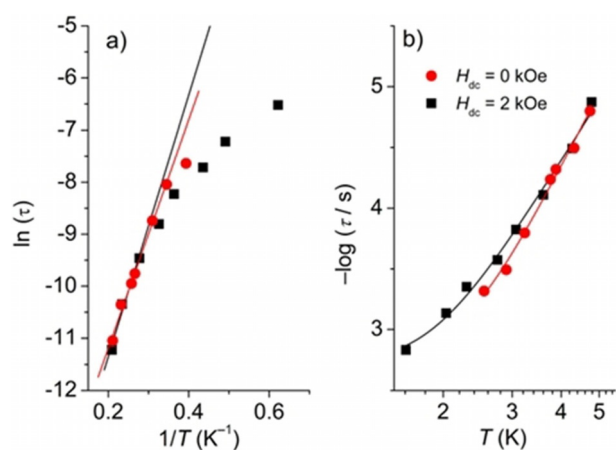

Figure 4. Relaxation time (τ) of **2** as a function of T in 0 kOe (red circles) and 2 kOe (black squares) external fields. Panel (a) shows the best-fit of the high-temperature region to the Arrhenius equation, that is, assuming exclusive operation of the Orbach relaxation process. Panel (b) shows the best-fit of all data points using a combination of quantum tunnelling and Raman processes.

cannot explain the relaxation behaviour. This hypothesis is also supported by the frequent observation that the experimental U_{eff} is significantly lower than the energy gap between the ground and first excited states.[3,18] One reason for the non-lin-

earity of the Arrhenius plot is the contribution of other relaxation mechanisms, such as quantum tunnelling, direct relaxation and Raman processes. In fact, in many lanthanide and actinide complexes, it has been observed that the Orbach process via a real intermediate state is just a small contribution to the relaxation.[45–47]

These possible relevant contributions to the relaxation in **2** can be described by Equation (1):[2, 3, 13, 38–40]

$$\tau^{-1} = \tau_{QTM}^{-1} + AT + CT^n + \tau_0^{-1}\exp\left(-\frac{U_{eff}}{k_B T}\right) \qquad (1)$$

in which τ_{QTM}^{-1}, A, C and τ_0 terms describe the quantum tunnelling, direct relaxation, Raman process and Orbach process, respectively. For the Raman process in Kramers ions, an exponent of $n = 9$ is predicted, although different values have been found in practice as a result of the inadequacy of the Debye model for the description of phonons in molecular solids.[7] The simplest model that led to an acceptable fit of all data points was a combination of the Raman and quantum tunnelling of the magnetization (QTM), processes (Figure 4 b, i.e., $A = \tau_0 = 0$). Table 1 lists the obtained parameters.

Table 1. Magnetic relaxation fit parameters for **2**.

Parameter	$H_{dc} = 0$ kOe	$H_{dc} = 2$ kOe
τ_{QTM}^{-1} [10^3 s^{-1}]	0.7(5)	6.2(6)
C [s^{-1} K^{-n}]	4(3)	20(8)
n	6.2(6)	5.1(3)

These parameters are in good agreement with those found for other actinide- and lanthanide-based single ion magnets (SIMs).[18, 45, 48, 49] However, the occurrence of any of these processes cannot be conclusively demonstrated. Also, the Debye model of phonon densities has been shown to be inapplicable to molecular complexes, and a dominant role of molecular vibrations in the relaxation process has been reported.[7, 50, 51] Thus, both the vibrational spectrum and the electronic structure must be studied in detail.

Theoretical calculations

For a first insight into the electronic structure of **2**, multi-reference ab initio calculations based on the experimental crystal structure were performed. A configuration-averaged Hartree–Fock (CAHF) calculation was employed to obtain averaged orbitals (Table S3, Supporting Information),[52] where local density fitting approximation was exploited to speed up the calculation process.[53, 54] Subsequently, the electronic Hamiltonian and spin-orbit operator were diagonalized in this basis, yielding the energy spectrum and eigenstates shown in Figure 5 and Table S4 (Supporting Information). The energy-level diagram clearly reveals groups of states that can be assigned to the Russell–Saunders multiplets ^4I_J ($J = 9/2$ to $15/2$ in order of increasing energy). In view of the large spin-orbit coupling and
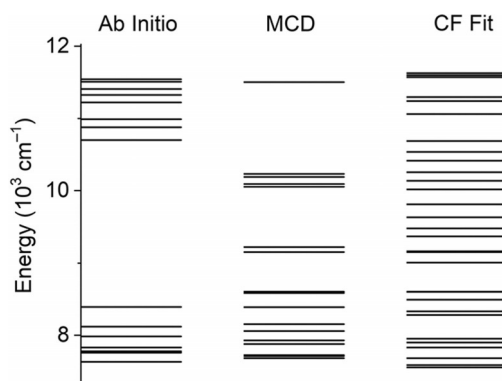

Figure 5. Experimental and calculated energy-level diagrams (expanded scale) for **2**, up to 12 000 cm^{-1} (CF = crystal field).

substantial covalency, J is not necessarily a good quantum number. For aiding the crystal field fit of the experimental excitation energies, the compound was also symmetrized to C_3. Analogous calculations starting from this idealized structure were performed. The results are qualitatively very similar, and are discussed below. Projection of the two lowest states calculated for the real structure onto a pseudo-spin 1/2 yields the following principal g-tensor components for this Kramers doublet (KD): $g_1 = 3.546$, $g_2 = 2.638$ and $g_3 = 0.802$. This suggests a considerably mixed ground doublet of the lowest multiplet. Indeed, projection of the lowest 10 states onto a 9/2 pseudo-spin by means of the SINGLE ANISO program allows expressing the composition of the Kramers doublets in terms of m_J functions. The ab initio results for the symmetrized complex suggest that the ground Kramers doublet is largely composed of the $|\pm 1/2>$ m_J wave function, with smaller contributions of $|\pm 7/2>$ and $|\pm 5/2>$ (Table S5, Supporting Information). The first excited Kramers doublet was calculated to lie at 147 cm^{-1} above the ground doublet and essentially consist of a 50/50 mixture of $|\pm 9/2>$ and $|\pm 3/2>$ m_J. The fact that the first excited Kramers doublet was calculated to be at much higher energies than that of the U_{eff} found by the analysis of ac susceptibility is a clear indication that an energy-barrier picture for the relaxation of the magnetic moment may not be applicable here, as already suggested by the fits of the relaxation time. Figure 2 shows the calculated susceptibility and magnetization curves based on the ab initio calculations; the calculated values are larger than the experimental values.

Projection of the lowest energy levels on a 15/2 pseudo-spin allowed the extraction of crystal field parameters (Table S6, Supporting Information), which are used as initial guesses in the crystal field analysis (see below). To assess the influence of the size of the active space, it was expanded in a subsequent calculation to include 3 electrons in 19 orbitals, in which the latter were selected to include a further set of f-orbitals (double shell) and d orbitals.[55] The ensuing CASSCF (complete active space self-consistent field) calculation resulted in a slight decrease in the gap between the third and fourth multiplets (below and above 10 000 cm^{-1}, respectively, Figure S6, Supporting Information). It also gave slightly different g-tensor values for the ground KD (Table S7, Supporting Information)

and slightly different simulations of the susceptibility and magnetization curves (Figure S7, Supporting Information). Interestingly, the first two excited KDs of the ground multiplets were calculated at much lower energies than those in the original calculation (Table S3, Supporting Information), but the total crystal field splitting of the ground multiplet remains essentially constant. These results indicate that the ab initio calculations are not yet at their optimum and that other effects should be taken into account. These include even larger active spaces or dynamical correlations at the complete active space perturbation theory of second order (CASPT2) or multi-reference configuration interaction (MRCI) level. However, such calculations rapidly exceed current capabilities and indeed proved not to be feasible with the hardware available to us. This motivated us to probe the electronic structure in more detail by using a variety of spectroscopic techniques.

Spectroscopic analyses

Low-temperature high-frequency EPR (HFEPR) spectroscopy is a sensitive probe for the properties of the ground KD of f-element complexes.[46] HFEPR spectra recorded at frequencies between 180 and 370 GHz (Figure 6) display three sharp peaks in addition to a number of less defined features. We attribute the sharp features to the three principal components of the rhombic g-tensor of the ground KD of **2**. The additional features are ascribed to incomplete powder averaging in an imperfectly ground sample. In fact, these EPR lines are much sharper than those typically observed in HFEPR spectra of trivalent lanthanide complexes. We are not aware of any existing HFEPR spectroscopic studies of uranium(III), and reports of measurements at conventional frequencies are also scarce.[48,56–58] A linear fit of the resonance fields as a function of frequency for each of
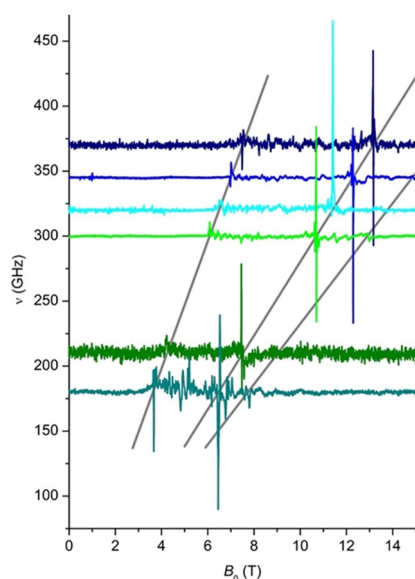
Figure 6. HFEPR spectra recorded on a pressed-powder sample of **2**, recorded at $T = 5$ K using several microwave frequencies (180–370 GHz). Grey lines indicate the three resonances due to the principal components of the g-tensor of the ground Kramers doublet.

the sharp peaks (Figure S8, Supporting Information) yielded the g-values of $g_1 = 3.54(5)$, $g_2 = 2.042(4)$ and $g_3 = 1.66(5)$, in which the g_1 value exactly matches that found in the ab initio calculations, whereas the other two values deviate significantly. Not too dissimilar values were found for $[U^{III}(N^{**})_3]$ $[N^{**} = N\text{-}(SiMe_2t\text{Bu})_2^-]$ ($g_{eff} = 3.55, 2.97$ and 0.553).[58]

In case transitions to the ground multiplet are observed, luminescence spectroscopy is an excellent technique for the experimental determination of the energy-level structure of this multiplet.[59–62] However, no luminescence spectrum could be obtained for **2**. Alternatively, far-infrared (FIR) spectroscopy can be used to precisely determine the energies of the first CF states of the ground multiplet.[46,63,64] The low-temperature FIR spectra (Figure 7 and S9, Supporting Information) are surpris-
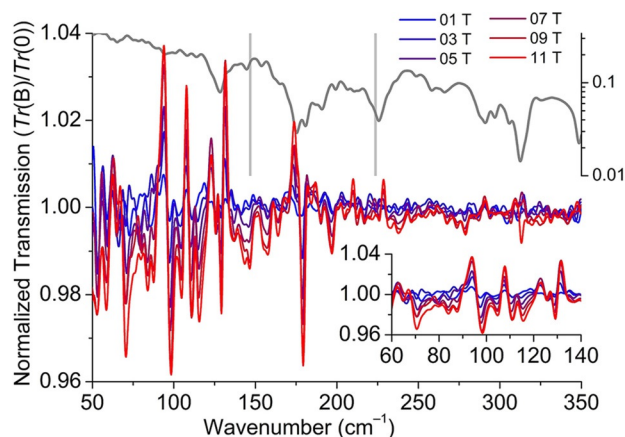
Figure 7. Normalized transmission spectra recorded on a pressed-powder pellet of **2** dispersed in eicosane (1:20) at $T = 4.2$ K and different fields as indicated. The grey spectrum is the absolute transmission spectrum at 0 T and 4.2 K. The inset expands the 60–140 cm^{-1} region, with the same axis units as in the main figure.

ingly rich. These spectra have been normalized by dividing them by the 0 T spectrum. Peaks pointing downward correspond to spectral density that appears upon application of a magnetic field, whereas those pointing upward correspond to spectral density that disappears. In the region up to 350 cm^{-1}, one distinct band at about 175 cm^{-1} and groups of bands around 100 and 130 cm^{-1} can be observed. Such rich spectra are typically not observed for lanthanides.[40,47,63] Similar features have been observed in four-coordinate cobalt complexes, and they were attributed to strong spin-phonon coupling.[65] As a consequence, excitations obtain mixed spin-phonon or vibronic character. Tentatively, the features around 100 cm^{-1} are assigned to an excitation with predominant spin character because the transmission spectrum (grey line in Figure 7) has no pronounced peak at that frequency (phonon transitions are much more intense than crystal field transitions on account of them being electric-dipole transitions). The features at approximately 130 cm^{-1} are attributed to excitations with mostly phonon/vibrational character. These spin excitation energies of 100 and 175 cm^{-1} are similar but not identical to the CF excitation energies of 147 and 224 cm^{-1}, calculated by ab initio

methods. Because of the tentative nature of these assignments, we decided to explore the energy spectrum in a broader range by means of optical spectroscopy. A subsequent fit of all the found energy levels may shed further light on the energetic structure of the ground multiplet.[46]

MCD spectroscopy in the UV/Vis/NIR spectral regions is a very powerful electronic spectroscopic technique for the f-elements.[46] Its power stems from the fact that the MCD is a signed quantity, which often allows the resolution of partially overlapping bands. In addition, the MCD effect increases with the magnetic moment, which leads to a relative intensity increase for (weak) f–f transitions compared to f–d transitions and charge-transfer transitions. The MCD spectra (Figure 8 and
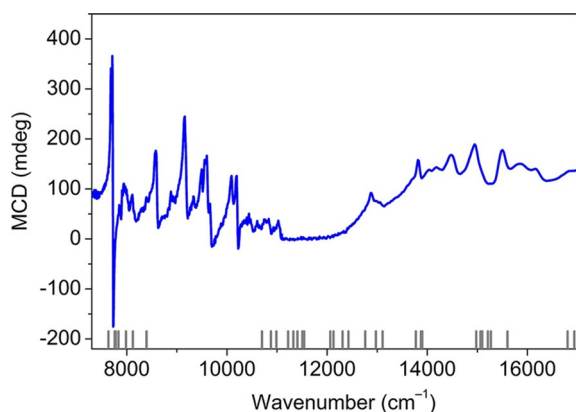

Figure 8. MCD spectrum of **2** in a silicone-grease mull recorded at $T = 1.5$ K and $B = 5$ T.

S10, Supporting Information) recorded at 1.5 K and 5 T display a set of sharp peaks between 7000 and 11 000 cm^{-1}, three broad bands at 15 000, 18 000 and 21 000 cm^{-1} (all with sharper peaks superimposed), as well as a weaker featureless band at about 34 000 cm^{-1}. The sharp peaks are attributed to 5f–5f transitions, whereas the broad bands are assigned to $5f^3 \rightarrow 5f^2 6d^1$ transitions.[66–68] Gaussian deconvolution allowed the extraction of 17 distinct excitation energies. Interestingly, in the experiment, peaks are observed well-spread in the region from 7000 to 11 000 cm^{-1}, whereas the ab initio calculations predict a distinct gap between groups of levels centred around 8000 and 11 000 cm^{-1}. The larger deviation of the energies of the higher-lying crystal field levels may be attributed to covalence effects of the more extended 5f orbitals with the ligand orbitals.[69]

Given this discrepancy between the ab initio and experimental energies, we sought to fit the experimental energies to a suitable Hamiltonian by using the semi-empirical CONDON program.[70] A suitable Hamiltonian for this purpose is $\widehat{H} = \widehat{H}_{FI} + \widehat{H}_{CF}$, where FI denotes the free ion, and CF denotes the effect of the crystal field generated by the ligands. The free-ion Hamiltonian consists of terms describing the effects of spin-orbit coupling and f-inter-electronic repulsion.[71] Here we have used the following starting values for the parameters included in the fit procedure: $\xi_{5f} = 1516$ cm^{-1}, $F^2 = 36 305$ cm^{-1}, $F^4 = 26 462$ cm^{-1} and $F^6 = 23 130$ cm^{-1}. The CF-Hamiltonian can

be expressed as Equation (2), in which C_k^q are tensor operators related to the spherical harmonics and B_k^q the crystal field parameters (CFPs).

$$
\widehat{H}_{CF} = \sum_{k=2,4,6} \left\{ B_{k0} C_0^k + \sum_{q=1}^{k} \left[B_{kq} \left(C_{-q}^k + (-1)^q C_q^k \right) + i B_{kq'} \left(C_{-q}^k - (-1)^q C_q^k \right) \right] \right\}
$$

(2)

In view of the limited number of experimental energies, we were constricted to idealize the symmetry of **2** to C_3. Ab initio calculations on a symmetrized structure revealed that the essential features of the CF splitting are not affected by symmetry idealization. This approximation implies that the only nonvanishing CFPs are B_{20}, B_{40}, B_{43}, $B_{43'}$, B_{60}, B_{63}, $B_{63'}$, B_{66} and $B_{66'}$. Then the calculated C_3-symmetrized set of CFPs was introduced into the CONDON package as an initial guess. The free-ion parameters were also varied with a few iterations in a second step. Once a satisfactory goodness-of-fit, SQX[70]

(SQX $= \sqrt{\left[\sum_{i=0}^{n} \frac{1}{\sigma_i} \left(1 - \frac{\chi_{\text{theo}}}{\chi_{\text{exptl}}} \right)^2 \right] / n}$, where χ_{theo} and χ_{exptl} are the

calculated and measured magnetic susceptibility, respectively, σ_i is a weighting factor, which as standard is 1, and n is the number of points included in the fit) of the MCD energy levels and HFEPR spectral data was achieved (collective SQX < 1%), the CFP set was refined, taking into account the magnetic susceptibility and magnetization data. The resulting full set of parameters and energy levels are given in Tables S4 and S6 (Supporting Information). The fitted magnetic susceptibility, which corresponds very well to the experimental data in all of the temperature range when corrected by a -3×10^{-4} emu mol^{-1} temperature-independent paramagnetism, is plotted in Figure 2 (red line), together with the magnetization curve at 1.7 K (see Experimental Section for further details). The obtained SQX for the MCD energies is 1.16%, with a collective SQX of 0.65%. This notably improved our starting point, which had a deviation of 2.94% for the energies when using the full Hamiltonian.

According to this phenomenological description, the ground state is determined mainly by $| \pm 7/2 >$ (62%) and $|\mp 5/2 >$ (35%), with a very small contribution of $| \pm 1/2 >$ (3%). This description is compatible with the observed SMM behaviour. Compared with the ab initio results for the ground state, they coincide with the m_J components that are involved, but the composition is remarkably different. This is not surprising because in the fit we included the g_3 value determined by EPR (1.66(5)), which is almost twice the value of the one predicted by ab initio calculations (0.802), evidencing the presence of larger contributions of higher m_J microstates in the ground state. The mixed nature of the ground-state wave function may be attributed to the competition between both the equatorial (amino and amido) groups with the apical oxygen atom of the OPPh$_3$ group. According to the wave-function composition extracted from the phenomenological description (CONDON fit), the inclusion of the apical group may be the

key to stabilizing a ground state composed mainly of higher m_J microstates but not necessarily sufficient to achieve *easy axis* instead of *easy plane* anisotropy. The effect of this apical group appears to be underestimated by the ab initio calculations, yielding a dominant effect of the equatorial amino and amido groups. To treat the apical ligand field generated by the $OPPh_3$ group properly, dynamical correlation must be included in the calculation, for example, by means of CASPT2 or MRCI. However, such calculations exceed current capacities. Regarding the crystal field parameters, all three diagonal CFPs are larger in magnitude than the ab initio calculated values, which results in an overall ligand field splitting of the ground multiplet $J=9/2$ of about $1246\ cm^{-1}$. Consequently, this is about 40% larger than the total ligand field splitting determined by ab initio calculations (865 and $872\ cm^{-1}$ for the real and C_3-symmetrized structures, respectively). In contrast, the first excited Kramers doublet is located at about $142\ cm^{-1}$, which is very close to the value predicted using the real structure ($147\ cm^{-1}$) and is compatible with the experimental data. Also, the first excited multiplet ($J=11/2$) is calculated at $3847\ cm^{-1}$, which is in good agreement with the ab initio results. However, this picture clearly differs for the upper part of the energy-level diagram: from the CF fit, a large number of energy levels are obtained (Figure 5, and Figure S5) that are not all observed in the MCD experiment. Interestingly, the CF fit also suggests a continuous series of energy levels, in agreement with the MCD results but in contrast to the ab initio calculations.

Conclusion

We have successfully prepared and characterized a uranium complex, $[U^{III}(\{SiMe_2NPh\}_3\text{-tacn})(OPPh_3)]$ (**2**), that shows single-ion magnetic behaviour, in contrast to its closely related precursor **1**, which is a rare example of a uranium(III) compound with no evidence for slow relaxation at low temperatures. The intuitive explanation for this difference is that the axial $OPPh_3$ ligand stabilizes large m_J states. However, the present multi-technique experimental and theoretical investigation shows that the observed different behaviour cannot be related to the different crystal fields in a straightforward manner. These results, which illustrate the challenges of crystal field engineering in actinides, constitute a solid first step toward the rational development of actinide single-molecule magnets.

Experimental Section

Synthesis: $U^{III}[(\{SiMe_2NPh\}_3\text{-tacn})(OPPh_3)]$ (**2**) was prepared by reacting the precursor (**1**) with an equimolar amount of triphenylphosphine oxide in toluene by an adduct-formation reaction, following a route mentioned in the Supporting Information (Scheme S1) of a previous publication of one of us.[31] Dark-red crystals of **2** were obtained from a concentrated solution of compound **2** in toluene. Yield: 61 mg (58%); elemental analysis calcd (%) for $C_{62}H_{76}N_6OPSi_3U$ (1274.57): C 58.42, H 6.01, N 6.59; found: C 58.09, H 6.11, N 6.66.

Magnetometric measurements: Magnetometric measurements of **2** were carried out on crystalline powder samples embedded in *n*-hexane. Due to their pronounced air sensitivity, the samples were sealed under vacuum inside a quartz tube. Magnetization was measured with a 6.5 T S700X SQUID magnetometer (Cryogenic Ltd.) in the temperature range 1.8–300 K at several magnetic fields. The paramagnetic susceptibility was obtained after correction for the core diamagnetism estimated from Pascal's constants as $-5.58\times10^{-4}\ emu\,mol^{-1}$. At low temperatures (1.7–10 K), ac susceptibility measurements were obtained with a MagLab 2000 system (Oxford Instruments) with an ac field of 5 Oe in the frequency range 10 Hz–10 kHz, in 0 and 2000 G fields. Isothermal measurements, between 1.6 and 5 K, were performed in the 10 Hz–10 kHz frequency range. At the lowest temperature (1.8 K), additional $\chi_{ac}=f(\omega)$ measurements were also performed, in several static (dc) fields up to 5 kOe

FIR spectroscopy: FIR spectra were recorded on a Bruker IFS 66v/s FTIR spectrometer with a globar source and a composite bolometer detector element located inside an 11 T magnet directly below the sample. Samples consisted of 10 mm pressed powder pellets.

MCD spectroscopy: MCD spectra were recorded on mulls of the solid compounds in transparent vacuum grease with an Aviv 42 CD spectrometer equipped with an Oxford Instruments Spectromag 10 T optical cryomagnet and photomultiplier and InGaAs detectors.

HFEPR spectroscopy: HFEPR powder spectra were recorded with a home-built spectrometer.[72] The radiation source (0–20 GHz signal generator, Anritsu) was combined with an amplifier-multiplier chain (VDI) to obtain the desired frequencies. It featured a quasi-optical bridge (Thomas Keating) and induction-mode detection. The detector was a QMC magnetically tuned InSb hot-electron bolometer. The magnet was an Oxford cryomagnet (15/17 T) equipped with a variable-temperature inset (1.5–300 K).

Multi-reference ab initio calculations: The ab initio calculations were performed with the Molpro suite of programs.[73,74] The calculations followed the published LDF-CAHF+CASCI/SI-SO (local-density-fitted configuration-averaged Hartree–Fock + complete active space configuration interaction followed by state-interaction through spin-orbit coupling).[53,54] The active space consisted of three electrons in the seven 5f-like orbitals.

Crystal field modelling: The results of the ab initio calculations were used as a starting point to phenomenologically describe the spectroscopic and static magnetic properties of the complex using the full basis of microstates in the latest version of the CONCORD code, which is part of the CONDON package.[70] The non-negligible crystal field parameters of the C_3-symmetrized ab initio calculations (B_{20}, B_{40}, B_{43}, $B_{43'}$, B_{60}, B_{63}, $B_{63'}$, B_{66}, $B_{66'}$) were used as initial input. The MCD spectra and the magnetic data were fitted simultaneously in a two-step procedure, also taking into account the high-frequency EPR data. The χT product was simulated using the CONDON package, and the magnetization curve at low temperature was simulated by projecting the CF parameters on the ground multiplet.

Crystallographic data: CCDC 299439 (**2**) contains the supplementary crystallographic data for this paper. These data are provided free of charge by The Cambridge Crystallographic Data Centre.

Acknowledgements

Conflict of interest

The authors declare no conflict of interest.

[1] D. N. Woodruff, R. E. Winpenny, R. A. Layfield, *Chem. Rev.* **2013**, *113*, 5110–5148.

[2] S. T. Liddle, J. van Slageren, *Chem. Soc. Rev.* **2015**, *44*, 6655–6669.

[3] S. G. McAdams, A.-M. Ariciu, A. K. Kostopoulos, J. P. Walsh, F. Tuna, *Coord. Chem. Rev.* **2017**, *346*, 216–239.

[4] L. Escalera-Moreno, J. J. Baldoví, A. Gaita-Ariño, E. Coronado, *Chem. Sci.* **2018**, *9*, 3265–3275.

[5] N. Ishikawa, M. Sugita, T. Ishikawa, S. Koshihara, Y. Kaizu, *J. Am. Chem. Soc.* **2003**, *125*, 8694–8695.

[6] Y. S. Ding, N. F. Chilton, R. E. Winpenny, Y. Z. Zheng, *Angew. Chem.* **2016**, *55*, 16071–16074; *Angew. Chem.* **2016**, *128*, 16305–16308.

[7] F.-S. Guo, B. Day, Y.-C. Chen, M.-L. Tong, A. Mansikkamäki, R. A. Layfield, *Angew. Chem. Int. Ed.* **2017**, *56*, 11445–11449; *Angew. Chem.* **2017**, *129*, 11603–11607; C. A. Goodwin, F. Ortu, D. Reta, N. F. Chilton, D. P. Mills, *Nature* **2017**, *548*, 439.

[8] F.-S. Guo, B. M. Day, Y.-C. Chen, M.-L. Tong, A. Mansikkamäki, R. A. Layfield, *Science* **2018**, DOI: https://doi.org/10.1126/science.aav0652.

[9] Y.-C. Chen, J.-L. Liu, L. Ungur, J. Liu, Q.-W. Li, L.-F. Wang, Z.-P. Ni, L. F. Chibotaru, X.-M. Chen, M.-L. Tong, *J. Am. Chem. Soc.* **2016**, *138*, 2829–2837.

[10] S. Demir, J. M. Zadrozny, M. Nippe, J. R. Long, *J. Am. Chem. Soc.* **2012**, *134*, 18546–18549.

[11] S. Demir, M. Nippe, M. I. Gonzalez, J. R. Long, *Chem. Sci.* **2014**, *5*, 4701–4711.

[12] S. Demir, I.-R. Jeon, J. R. Long, T. D. Harris, *Coord. Chem. Rev.* **2015**, *289*, 149–176.

[13] J. D. Rinehart, M. Fang, W. J. Evans, J. R. Long, *J. Am. Chem. Soc.* **2011**, *133*, 14236–14239.

[14] S. A. Kozimor, B. M. Bartlett, J. D. Rinehart, J. R. Long, *J. Am. Chem. Soc.* **2007**, *129*, 10672–10674.

[15] L. Salmon, P. Thuéry, E. Rivière, J.-J. Girerd, M. Ephritikhine, *Dalton Trans.* **2003**, 2872–2880.

[16] L. Salmon, P. Thuéry, E. Rivière, M. Ephritikhine, *Inorg. Chem.* **2006**, *45*, 83–93.

[17] T. Le Borgne, E. Rivière, J. Marrot, P. Thuéry, J. J. Girerd, M. Ephritikhine, *Chem. Eur. J.* **2002**, *8*, 773–783.

[18] K. R. Meihaus, J. R. Long, *Dalton Trans.* **2015**, *44*, 2517–2528.

[19] S. T. Liddle, J. van Slageren in *Molecular Magnetism (*Eds. R. A. Layfield, M. Murugesu), Wiley-VCH, **2015**, pp. 315–336.

[20] L. Chatelain, J. P. Walsh, J. Pécaut, F. Tuna, M. Mazzanti, *Angew. Chem. Int. Ed.* **2014**, *53*, 13434–13438; *Angew. Chem.* **2014**, *126*, 13652–13656.

[21] L. Chatelain, J. Pécaut, F. Tuna, M. Mazzanti, *Chem. Eur. J.* **2015**, *21*, 18038–18042.

[22] V. Mougel, L. Chatelain, J. Pécaut, R. Caciuffo, E. Colineau, J.-C. Griveau, M. Mazzanti, *Nat. Chem.* **2012**, *4*, 1011–1017.

[23] V. Mougel, L. Chatelain, J. Hermle, R. Caciuffo, E. Colineau, F. Tuna, N. Magnani, A. de Geyer, J. Pécaut, M. Mazzanti, *Angew. Chem. Int. Ed.* **2014**, *53*, 819–823; *Angew. Chem.* **2014**, *126*, 838–842.

[24] D. King, D. M. King, P. A. Cleaves, A. J. Wooles, B. M. Gardner, N. F. Chilton, F. Tuna, W. Lewis, E. J. L. McInnes, S. T. Liddle, *Nat. Commun.* **2016**, *7*, 13773.

[25] C. Apostolidis, A. Morgenstern, J. Rebizant, B. Kanellakopulos, O. Walter, B. Powietzka, M. Karbowiak, H. Reddmann, H. D. Amberger, *Zeitschr. Anorg. Allg. Chem.* **2010**, *636*, 201–208.

[26] M. A. Antunes, J. T. Coutinho, I. C. Santos, J. Marçalo, M. Almeida, J. J. Baldoví, L. C. Pereira, A. Gaita-Ariño, E. Coronado, *Chem. Eur. J.* **2015**, *21*, 17817–17826.

[27] F. Moro, D. P. Mills, S. T. Liddle, J. van Slageren, *Angew. Chem. Int. Ed.* **2013**, *52*, 3430–3433; *Angew. Chem.* **2013**, *125*, 3514–3517.

[28] J. D. Rinehart, J. R. Long, *Chem. Sci.* **2011**, *2*, 2078–2085.

[29] J. J. Baldoví, S. Cardona-Serra, J. M. Clemente-Juan, E. Coronado, A. Gaita-Ariño, A. Palii, *Inorg. Chem.* **2012**, *51*, 12565–12574.

[30] J. Sievers, *Z. Phys. B Condens. Matter* **1982**, *45*, 289–296.

[31] M. A. Antunes, M. Dias, B. Monteiro, Â. Domingos, I. C. Santos, N. Marques, *Dalton Trans.* **2006**, 3368–3374.

[32] B. Monteiro, D. Roitershtein, H. Ferreira, J. R. Ascenso, A. M. Martins, Â. Domingos, N. Marques, *Inorg. Chem.* **2003**, *42*, 4223–4231.

[33] H. Yin, A. J. Lewis, U. J. Williams, P. J. Carroll, E. J. Schelter, *Chem. Sci.* **2013**, *4*, 798–805.

[34] J. G. Brennan, R. A. Andersen, A. Zalkin, *Inorg. Chem.* **1986**, *25*, 1761–1765.

[35] J.-C. Berthet, M. Nierlich, M. Ephritikhine, *Polyhedron* **2003**, *22*, 3475–3482.

[36] L. Maria, Â. Domingos, A. Galvão, J. Ascenso, I. Santos, *Inorg. Chem.* **2004**, *43*, 6426–6434.

[37] S. T. Liddle, *Angew. Chem. Int. Ed.* **2015**, *54*, 8604–8641; *Angew. Chem.* **2015**, *127*, 8726–8764.

[38] N. M. Edelstein, J. Goffart, J. Katz, *Radiochemistry and Nuclear Chemistry*, Butterworth-Heinemann, Woburn, **1986**, pp. 327–329.

[39] D. R. Kindra, W. J. Evans, *Chem. Rev.* **2014**, *114*, 8865–8882.

[40] N. M. Edelstein, J. Fuger, J. J. Katz, L. R. Morss, in *The Chemistry of the Actinide and Transactinide Elements*, Springer, Heidelberg, **2010**, pp. 1753–1835.

[41] J. T. Coutinho, M. A. Antunes, L. C. Pereira, J. Marçalo, M. Almeida, *Chem. Commun.* **2014**, *50*, 10262–10264.

[42] J. T. Coutinho, M. A. Antunes, L. C. Pereira, H. Bolvin, J. Marçalo, M. Mazzanti, M. Almeida, *Dalton Trans.* **2012**, *41*, 13568–13571.

[43] N. Magnani, *Int. J. Quantum Chem.* **2014**, *114*, 755–759.

[44] J. D. Rinehart, J. R. Long, *J. Am. Chem. Soc.* **2009**, *131*, 12558–12559.

[45] E. Lucaccini, L. Sorace, M. Perfetti, J.-P. Costes, R. Sessoli, *Chem. Commun.* **2014**, *50*, 1648–1651.

[46] Y. Rechkemmer, J. E. Fischer, R. Marx, M. A. Dörfel, P. Neugebauer, S. Horvath, M. Gysler, T. Brock-Nannestad, W. Frey, M. F. Reid, *J. Am. Chem. Soc.* **2015**, *137*, 13114–13120.

[47] S. Gómez-Coca, A. Urtizberea, E. Cremades, P. J. Alonso, A. Camón, E. Ruiz, F. Luis, *Nat. Commun.* **2014**, *5*, 4300.

[48] K. R. Meihaus, S. G. Minasian, W. W. Lukens Jr, S. A. Kozimor, D. K. Shuh, T. Tyliszczak, J. R. Long, *J. Am. Chem. Soc.* **2014**, *136*, 6056–6068.

[49] M. Gregson, N. F. Chilton, A.-M. Ariciu, F. Tuna, I. F. Crowe, W. Lewis, A. J. Blake, D. Collison, E. J. McInnes, R. E. Winpenny, *Chem. Sci.* **2016**, *7*, 155–165.

[50] A. Lunghi, F. Totti, R. Sessoli, S. Sanvito, *Nat. Commun.* **2017**, *8*, 14620.

[51] A. Lunghi, F. Totti, S. Sanvito, R. Sessoli, *Chem. Sci.* **2017**, *8*, 6051–6059.

[52] W. Van den Heuvel, S. Calvello, A. Soncini, *Phys. Chem. Chem. Phys.* **2016**, *18*, 15807–15814.

[53] P. P. Hallmen, C. Köppl, G. Rauhut, H. Stoll, J. van Slageren, *J. Chem. Phys.* **2017**, *147*, 164101–164110.

[54] C. Köppl, H.-J. Werner, *J. Chem. Theory Comput.* **2016**, *12*, 3122–3134.

[55] L. Ungur, L. F. Chibotaru, *Chem. Eur. J.* **2017**, *23*, 3708–3718.

[56] J. Seed, S. Liddle, M. Gregson, F. Tuna, N. Chilton, A. Wooles, E. McInnes, *Angew. Chem. Int. Ed.* **2017**, *129*, 11534–11538; *Angew. Chem.* **2017**, *129*, 11692–11696.

[57] W. W. Lukens, M. Speldrich, P. Yang, T. Duignan, J. Autschbach, P. Kögerler, *Dalton Trans.* **2016**, *45*, 11508–11521.

[58] C. A. Goodwin, F. Tuna, E. J. McInnes, S. T. Liddle, J. McMaster, I. J. Vitorica-Yrezabal, D. P. Mills, *Chem. Eur. J.* **2014**, *20*, 14579–14583.

[59] M. A. Sørensen, U. B. Hansen, M. Perfetti, K. S. Pedersen, E. Bartolomé, G. G. Simeoni, H. Mutka, S. Rols, M. Jeong, I. Zivkovic, M. Retuerto, A. Arauzo, J. Bartolomé, S. Piligkos, H. Weihe, L. H. Doerrer, J. van Slageren, H. M. Rønnow, K. Lefmann, J. Bendix, *Nat. Commun.* **2018**, *9*, 1292.

[60] J. Long, Y. Guari, R. A. Ferreira, L. D. Carlos, J. Larionova, *Coord. Chem. Rev.* **2018**, *363*, 57–70.

[61] Y. Bi, C. Chen, Y.-F. Zhao, Y.-Q. Zhang, S.-D. Jiang, B.-W. Wang, J.-B. Han, J.-L. Sun, Z.-Q. Bian, Z.-M. Wang, *Chem. Sci.* **2016**, *7*, 5020–5031.

[62] L. Norel, L. E. Darago, B. Le Guennic, K. Chakarawet, M. I. Gonzalez, J. H. Olshansky, S. Rigaut, J. R. Long, *Angew. Chem. Int. Ed.* **2018**, *57*, 1933 – 1938; *Angew. Chem.* **2018**, *130*, 1951 – 1956.

[63] R. Marx, F. Moro, M. Dörfel, L. Ungur, M. Waters, S.-D. Jiang, M. Orlita, J. Taylor, W. Frey, L. Chibotaru, *Chem. Sci.* **2014**, *5*, 3287 – 3293.

[64] M. Gysler, F. El Hallak, L. Ungur, R. Marx, M. Hakl, P. Neugebauer, Y. Rechkemmer, Y. Lan, I. Sheikin, M. Orlita, J. van Slageren, *Chem. Sci.* **2016**, *7*, 4347 – 4354.

[65] Y. Rechkemmer, F. D. Breitgoff, M. Van Der Meer, M. Atanasov, M. Hakl, M. Orlita, P. Neugebauer, F. Neese, B. Sarkar, J. Van Slageren, *Nat. Commun.* **2016**, *7*, 10467 – 10475.

[66] I. Grenthe, J. Drożdżyński, T. Fujino, E. C. Buck, T. E. Albrecht-Schmitt, S. T. Wolf in *The Chemistry of the Actinide and Transactinide Elements (Volumes 1 – 5)*, (Eds. L. R. Morss, N. Edelstein, J. Fuger, J. J. Katz), Springer Science & Business Media, **2007**, pp. 253 – 698.

[67] J. Drożdżyński, *Coord. Chem. Rev.* **2005**, *249*, 2351 – 2373.

[68] D. P. Mills, F. Moro, J. McMaster, J. Van Slageren, W. Lewis, A. J. Blake, S. T. Liddle, *Nat. Chem.* **2011**, *3*, 454 – 460.

[69] A. Formanuik, A.-M. Ariciu, F. Ortu, R. Beekmeyer, A. Kerridge, F. Tuna, E. J. McInnes, D. P. Mills, *Nat. Chem.* **2016**, *9*, 578.

[70] J. van Leusen, M. Speldrich, H. Schilder, P. Kögerler, *Coord. Chem. Rev.* **2015**, *289*, 137 – 148.

[71] H.-D. Amberger, H. Reddmann, *Z. Anorg. Allg. Chem.* **2009**, *635*, 291 – 296.

[72] P. Neugebauer, D. Bloos, R. Marx, P. Lutz, M. Kern, D. A. Aguilà, J. Vaverka, O. Laguta, C. Dietrich, R. Clerac, *Phys. Chem. Chem. Phys.* **2018**, *20*, 15528 – 15534.

[73] H. J. Werner, P. J. Knowles, G. Knizia, F. R. Manby, M. Schütz, *Wiley Interdiscip. Rev.: Comput. Mol. Sci.* **2012**, *2*, 242 – 253.

[74] H. Werner, P. Knowles, G. Knizia, F. Manby, M. Schütz, P. Celani, W. Györffy, D. Kats, T. Korona, R. Lindh, A. Mitrushenkov, G. Rauhut, K. Shamasundar, T. Adler, R. Amos, A. Bernhardsson, A. Berning, D. Cooper, M. Deegan, A. Dobbyn, F. Eckert, E. Goll, C. Hampel, A. Hesselmann, G. Hetzer, T. Hrenar, G. Jansen, C. Köppl, Y. Liu, A. Lloyd, R. Mata, A. May, S. McNicholas, W. Meyer, M. Mura, A. Nicklass, D. O'Neill, P. Palmieri, D. Peng, K. Pflüger, R. Pitzer, M. Reiher, T. Shozaki, H. Stöll, A. Stone, R. Tarroni, T. Thorsteinsson, M. Wang, *MOLPRO, version 2012.1*, a package of ab initio programs.